electronics

MDPI

Article

Semi-Analytical Approach versus Finite Element Method for Analysis of Propagation Properties in Rectangular Waveguides: Silica-Titania Technological Platform

Bartosz Janaszek [1,2,*], Muhammad A. Butt [1] and Ryszard Piramidowicz [1]

[1] Institute of Microelectronics and Optoelectronics, Warsaw University of Technology, Koszykowa 75, 00-662 Warsaw, Poland
[2] National Institute of Telecommunications, Szachowa 1, 04-894 Warsaw, Poland
* Correspondence: bartosz.janaszek@pw.edu.pl

Abstract: This work explicitly demonstrates a semi-analytical effective index approximation (EIA) approach for the description of the propagation properties of rib and ridge waveguides. By using the example of waveguides realized on a low-cost silica-titania (SiO_2:TiO_2) technological platform, we present that EIA may be successfully applied for the approximate determination of modal effective indices and single mode propagation conditions. All obtained results have been confirmed to be convergent with the finite element method (FEM) simulations at low relative error. Due to the tremendously fast execution time of EIA simulations in comparison with the FEM solver, we believe that the presented approach may be applied in a preliminary step of designing functional blocks in new and existing photonic integrated circuit technologies, which often require complex and multi-parameter calculations.

Keywords: silica-titania platform; effective index approximation; finite element method; optical waveguide

check for updates

Citation: Janaszek, B.; Butt, M.A.; Piramidowicz, R. Semi-Analytical Approach versus Finite Element Method for Analysis of Propagation Properties in Rectangular Waveguides: Silica-Titania Technological Platform. *Electronics* **2024**, *13*, 73. https://doi.org/10.3390/electronics13010073

Academic Editors: Elias Stathatos and Spyros N. Yannopoulos

Received: 5 December 2023
Revised: 15 December 2023
Accepted: 21 December 2023
Published: 22 December 2023

Copyright: © 2023 by the authors. Licensee MDPI, Basel, Switzerland. This article is an open access article distributed under the terms and conditions of the Creative Commons Attribution (CC BY) license (https://creativecommons.org/licenses/by/4.0/).

1. Introduction

Unlike their electronic counterparts, photonic integrated circuits (PICs) employ guided waves instead of electric signals to transport information [1]. The transition to the optical domain shows great promise in ultrafast data processing, which potentially may circumvent the power density limitations of highly integrated electronic circuits [2,3]. The advancement of photonic integrated circuits in recent years has also demonstrated the possibility of employing them in practical and novel applications, such as chip-scale signal processing [4], communications [2], versatile sensing [5,6] or quantum computing [7,8].

Over the past few decades, the development of simple, cost-effective and reliable technology for mass production of PIC elements and systems has been the objective of many researchers around the world [9–12]. In recent years, more and more attention has been put on alternatives to PIC mainstream technologies. In particular, the silica-titania (SiO_2:TiO_2) optical waveguide platform has been demonstrated to be operational in several practical applications [13–15]. What is more, it has been proven that by including a sol-gel waveguide film procurement and direct nanoimprinting of the waveguide pattern, the silica-titania material platform may offer precise tuning of the refractive index and thickness of the waveguide film while being substantially less expensive than mainstream PIC technologies [16,17].

The basic building block of PICs, which provides a means for signal transportation, is undoubtedly an optical waveguide. Most commonly, optical waveguides are classified into two classes: planar revealing optical confinement in one transverse direction and non-planar providing 2D transverse mode confinement. Typically, due to innate properties of

planar technologies, the photonic integrated circuits deploy the latter kind with rectangular-like transverse geometry, such as rib or ridge waveguides. Unfortunately, the description of light propagation, and thus designing new components based on rectangular waveguides, is complex and, in contrast to planar waveguides, cannot be performed via the use of exact analytical methods.

The horizon of PIC technology shines with unparalleled promise, poised to redefine industries through its cutting-edge capabilities. Progressing into the future, PICs are set to assume a central role in meeting the escalating demand for high-speed data communication and processing [18]. By seamlessly integrating multiple photonic functions on a single chip, these circuits usher in heightened efficiency, diminished power consumption, and expanded bandwidth, surpassing the capacities of conventional electronic circuits. The scope of PIC technology applications is expansive, encompassing domains from telecommunications and data centers to healthcare and sensing devices [19,20]. In the realm of telecommunications, PICs are primed to facilitate swifter and more dependable data transmission, while in data centers, they promise heightened performance coupled with enhanced energy efficiency. Furthermore, the versatility of PICs extends into cutting-edge fields like quantum computing [21] and LiDAR systems [22]. As the momentum of research and development propels us forward, the future of PIC technology emerges as a beacon of transformative potential, reshaping how we process and transmit information and ushering in a new era of efficiency and innovation across diverse sectors.

Presently, the design of PICs relies on a meticulous selection of predefined functional blocks featuring pre-established geometries tailored to existing technological platforms like SOI, SiN, and InP. Consequently, introducing a new material platform presents a formidable challenge, demanding not only advancements in technological processes but also the redefinition and rescaling of all functional blocks. Given that the design process often entails numerous iterations, employing electromagnetic solvers—known for their high computational demands—can significantly extend the time required for completion. To address that problem, semi-analytical methods that have been developed at an early stage of the optical waveguide simulation [23,24], may be applied to deliver accurate results with high speed and parametrization over a large number of variables.

In this study, we introduce a novel and highly effective index approximation (EIA) designed to serve as a rapid and dependable tool for the design and simulation of propagation properties in rectangular waveguides. The remarkably low approximation error has been validated through its excellent convergence with numerical results obtained using commercially available software. Using waveguides implemented on a cost-effective SiO_2:TiO_2 technological platform as an illustrative example, we showcase the successful application of the EIA approach in designing both ridge and rib waveguides, which are most commonly employed in practical PIC systems.

Our findings demonstrate that the proposed approach enables efficient parameterized simulations, facilitating a swift yet comprehensive analysis of propagation properties and the identification of single-mode propagation conditions within the specified material platforms. The versatility of the presented method allows for seamless adaptation to various types of rectangular waveguides, including buried, strip-loaded, or metamaterial waveguides. This versatility, coupled with its demonstrated accuracy, positions the EIA as a valuable and adaptable tool for advancing the design and understanding of rectangular waveguide systems.

2. Effective Index Approximation (EIA) Approach

In this section, we expound upon the theoretical underpinnings of the semi-analytical method under consideration. The initial segment of this section delves into an exact analytical elucidation of propagation in planar waveguides. Subsequently, the second part introduces an effective approach to describing propagation specifically in rib and ridge waveguides.

2.1. Propagation Properties of Planar Slab Dielectric Waveguide: Analytical Approach

The foundational element of integrated optical circuits, forming the basis for the approximate description of more sophisticated components, is a planar slab waveguide with infinite transverse dimensions, as illustrated in Figure 1. For our analysis, we assume that the light propagates in the z direction and that the media constituting the system are uniform in the y direction.

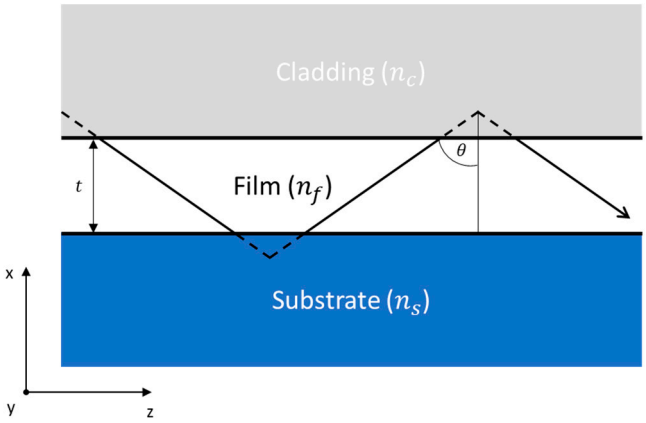

Figure 1. Ray optics model of wave propagation in slab waveguide.

The propagation of light in such a waveguide may explained via the use of an intuitive ray model according to which the guided wave follows a "zigzag" path and is reflected at the guiding film boundaries. The wave travelling in such a manner acquires phase change by passing through the film $kn_f t\cos\theta$, reflection from the bottom boundary $-2\varphi_c$, travelling again through the film $kn_f t\cos\theta$ and, finally, the reflection from the top boundary $-2\varphi_s$. Knowing that the total phase of the wave must be self-consisted, i.e., a multiple of 2π, we can formulate a transverse resonance or self-consistency condition.

$$2k_0 n_f t\cos\theta - 2\varphi_c - 2\varphi_s = 2m\pi, \tag{1}$$

where t is the guiding film thickness, k_0 is freespace wavevector and m is the integer denoting the mode order. The phase shift arising from total internal reflection at the boundaries can be derived from the Fresnel equations. The expression for this phase shift at the two interfaces under consideration is articulated as follows.

$$\varphi_c = a_{c(TE/TM)}\frac{\sqrt{n_f^2\sin^2\theta - n_c^2}}{n_f\cos\theta}, \tag{2}$$

$$\varphi_s = a_{s(TE/TM)}\frac{\sqrt{n_f^2\sin^2\theta - n_s^2}}{n_f\cos\theta}, \tag{3}$$

Note that, the phase shift at the boundary is polarization-dependent, i.e., $a_{c(TE)} = a_{s(TE)} = 1$ for TE polarization and $a_{TM(c)} = \frac{n_f^2}{n_c^2}$, $a_{TM(s)} = \frac{n_f^2}{n_s^2}$ for TM polarization of light. Due to its implicit nature, the exact solution of Equation (1) can be only obtained with the use of numerical methods for nonlinear root finding, such as the Newton–Raphson method. Thus for the given waveguide thickness t, the it can be solved numerically for $N_{eff} = n_f\sin\theta$, where $n_s + \varepsilon < N_{eff} < n_f - \varepsilon$ and $\varepsilon = 1e^{-10}$ define the search space. Hence, by solving Equation (1) at multiple points, we can derive the dispersion characteristics of the planar waveguide. These characteristics depict the effective index as a function of guiding film thickness for modes of various orders and polarization states (TE or TM).

2.2. Propagation Properties of Rectangular Waveguides: Semi-Analytical Approach

In practical integrated circuits, planar waveguides are rarely used; instead, waveguides of finite transverse dimensions, such as rib or ridge waveguides, that can confine light in finite cross-section geometry and, thus, allow a higher integration level are employed, see Figure 2a,b. Regrettably, deriving the exact analytical form of characteristic equations for waves propagating in waveguides with rectangular-like cross-sections proves to be an unattainable task. However, an approximate solution can be acquired with the use of characteristic equations for planar waveguides [25].

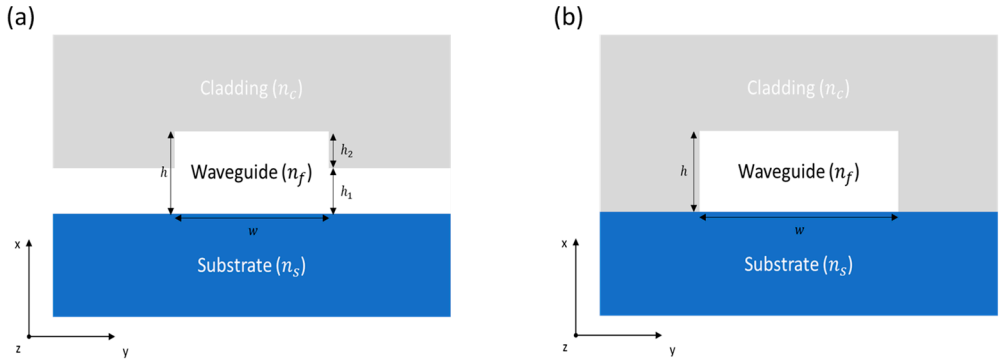

Figure 2. Schematic cross-section of rib (**a**) and ridge waveguide (**b**).

First, let us consider the case of a rib waveguide, for which the guidance conditions are provided as long as the "rib region", corresponds to the area with height $h = h_1 + h_2$, is sufficiently thick, which allows to obtain a larger effective index N_f then in the surrounding region, characterized by effective N_h index and physical thickness h_1, see Figure 3a.

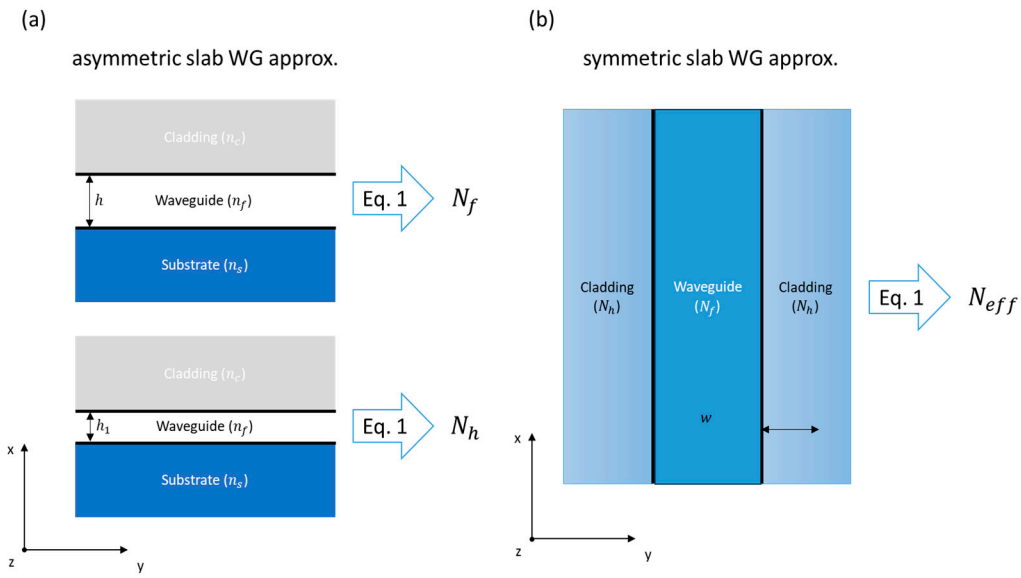

Figure 3. Graphical representation of conceptual slab waveguides used for calculation of effective refractive index in rib waveguide (**a**,**b**).

The effective indices N_f and N_h for the core and its surrounding area may be approximated by solving characteristic equations of the asymmetrical planar waveguide, see Equation (1), for two guiding film thicknesses, i.e., $t = h$ and $t = h_1$, and given mode order m in the x direction, see Figure 3a. Then, we can use the obtained effective indices N_f and N_h to determine effective guiding properties of rib waveguide. It is possible by substituting the guiding film and substrate/cladding indices with the effective indices in Equation (1), i.e., $n_f = N_f$ and $n_s = n_c = N_h$, and formulating a characteristic equation

for a symmetrical planar waveguide with thickness $t = w$ for the given mode order n in the y direction, see Figure 3b. The implicit equation obtained in this manner can be then solved by the use of well-established methods for nonlinear root finding, such as Newton–Raphson or Secant methods. Thus, via the use of this semi-analytical approach we can obtain the effective index $N_{eff(mn)}$ for the mode of given orders (m and n). It is worth underlining that the effective approach in the presented form is not suitable, i.e., may be burdened with significant error in comparison with numerical results, for rib waveguides with $h_1 < 0.5 \times h$, due to overestimated value of N_h obtained from planar waveguide approximation. However, such a problem does not exist in the case of ridge waveguide, for which the described approach may be applied by substituting the effective index of the surrounding layer with refractive index of the cladding, i.e., $N_h = n_c$, see Figure 2b. It is also worth underlining that, the effective modal index is searched within the range of $n_s + \varepsilon < N_{eff} < n_f - \varepsilon$, which may lead to errors in the determination of the cut-off width for the fundamental mode.

3. Results

The primary goal of this endeavor is to establish a robust and efficient simulation framework. This framework aims to function as a free and specialized alternative to commercially available software. Its purpose is to facilitate the design of integrated photonic circuits, particularly within a novel and cost-effective SiO_2:TiO_2 technological platform. This platform relies on sol-gel films and the direct nanoimprint technique, offering a unique and low-cost approach to integrated photonic circuitry design [26]. Thus, for our analysis, we have assumed material parameters corresponding to refractive indices of fused silica glass ($n_s = 1.4440$ @ λ_0 = 1.55 µm) [27], SiO_x:TiO_y composite ($n_f = 1.75645$ @ λ_0 = 1.55 µm) [28] and air ($n_c \approx 1$) [29]. Due to the technological constraints of the sol-gel technological framework, we have only considered waveguides of a height no larger than $h < 0.4$ µm . Additionally, to provide analysis of waveguides feasible within the frame of the considered technology, transverse dimensions, i.e., the waveguide width, have also been limited to values practically measurable employing realistic setups of light coupling, i.e., $a > 0.4$ µm for visible and $a > 1$ µm for infrared spectral range. Since single-mode propagation is typically of interest in optical signal transportation, we have concentrated on fundamental TE_0 mode propagation properties and corresponding multimodal cutoffs.

To validate the results obtained with our semi-analytical approach, we have performed numerical simulations by employing finite element method (FEM) via commercially available COMSOL Multiphysics 6.2 software. The FEM finds applications in the analysis and emulation of optical waveguides, which serve as conduits for manipulating and guiding light within a material. FEM serves as the means to address Maxwell's equations, the fundamental descriptions governing the propagation of electromagnetic waves, encompassing light.

Maxwell's equations form a comprehensive framework that establishes the intricate relationships among fundamental electromagnetic quantities. These include the electric charge density (ρ), the electric field (E), the electric displacement field (D), and the current (J). Additionally, the equations interconnect the magnetic field intensity (H) and the magnetic flux density (B). This elegant set of equations serves as the cornerstone for understanding the dynamic interplay between electric and magnetic fields, providing a profound foundation for the study and application of electromagnetism in diverse scientific and technological domains.

$$\nabla \cdot D = \rho \tag{4}$$

$$\nabla \cdot B = 0 \tag{5}$$

$$\nabla \times E = \frac{\partial}{\partial t} B \tag{6}$$

$$\nabla \times H = J + \frac{\partial}{\partial t} D \tag{7}$$

In the quest to unravel the intricacies encapsulated by Maxwell's equations, a solution necessitates the incorporation of a set of boundary conditions. Furthermore, the pursuit of understanding is deepened by integrating material constitutive relations, establishing connections between E and D, B and H as well as J and E. These pivotal relationships unfold within varying contexts, guided by specific assumptions and considerations. To navigate this intricate web of equations and conditions, diverse modules within the COMSOL product suite serve as invaluable tools. Through the seamless integration of these modules, solutions emerge as the equations harmoniously coupled with other physical phenomena. This holistic approach not only addresses the complexity inherent in electromagnetism but also facilitates a nuanced exploration of diverse scenarios and applications.

The optical waveguide's structural representation undergoes discretization, mirroring the conventional FEM practice, where the domain is subdivided into smaller elements. However, in the context of optical waveguides, the selection of the mesh is a critical consideration, as it must faithfully capture the geometric and material attributes of the waveguide. Common choices for element types encompass triangles or quadrilaterals for two-dimensional waveguides and tetrahedra or hexahedra for their three-dimensional counterparts. For the solution of the system of equations governing the electromagnetic field distribution, a range of numerical techniques is at one's disposal. These may encompass iterative solvers, direct solvers, or specialized algorithms tailored for eigenmode analysis. The culmination of this process yields valuable insights into the mode profiles and propagation characteristics inherent to the optical waveguide.

3.1. Rib Waveguides

Initiating our analysis, we delve into the propagation characteristics of the rib waveguide implemented within the SiO_2:TiO_2 technological platform under consideration (refer to Figure 2a). While the waveguide width traditionally takes center stage as the primary parameter of interest in the examination of rectangular waveguides, the case of rib waveguides introduces two additional crucial geometrical parameters: 'h'—representing the total height—and 'h_1'—signifying the surrounding layer height (as illustrated in Figure 2a).

Firstly, let us consider the influence of h_1 on modal effective index N_{eff} for fixed total height h = 0.4 µm. It is worth reiterating that for rib waveguides with $h_1 < 0.5 * h$, the presented method is not valid due to effective index overestimation. Thus, we have focused on the three following cases, i.e., h_1 = 0.25, 0.3, 0.35 µm . As we can see in Figure 4a, our method can be successfully used to calculate modal effective index as well as multimodal cut-off widths, i.e., waveguide widths for which the waveguide supports modes of higher orders (TE_{10} or TE_{01}) than fundamental mode (TE_{00}).

Numerical calculations, which may be treated as an exact solution, allow us to confirm that the proposed semi-analytical method reveals low effective index calculation error for all the considered parameters, i.e., below 0.7%, see Figure 4b. The considered error value has been calculated according to the definition of relative error, i.e., $|N_{EIM} - N_{FEM}|/N_{FEM}$, where N_{EIM} and N_{FEM} are effective indices calculated via the use of the proposed EIA approach and numerical software, respectively. Additionally, by calculating dispersion characteristics for higher mode orders, i.e., TE_{10} and TE_{01}, were able to determine the cut-off for single-mode propagation. The cut-off width error has been determined in a similar way as previously. In this case, of the multimodal cut-off width calculations, a relatively high error can be observed, i.e., up to ~28% error, see Figure 4c. Notwithstanding the inherent relative error, the EIA approach can be employed to identify approximate conditions conducive to sustaining single-mode propagation in rib waveguides. Additionally, it is important to highlight that, for a constant total height 'h', the overall error diminishes notably as the height of the surrounding layer 'h_1' increases, as illustrated in Figure 4b,c. This underscores the potential for mitigating errors and enhancing the reliability of the EIA approach by adjusting the height of the surrounding layer in the design of rib waveguides.

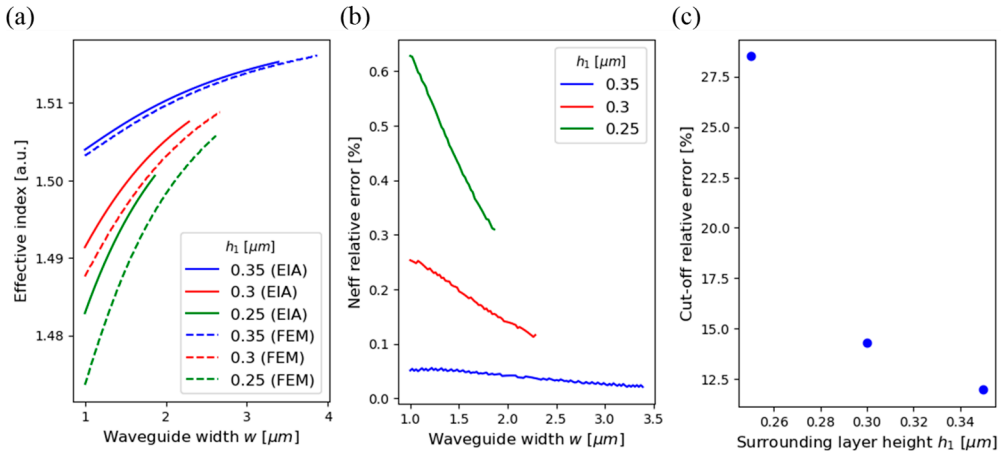

Figure 4. Effective index vs. waveguide width for rib waveguide of different surrounding layer height, where solid curve corresponds to semi-analytical and dashed to numerical calculations (**a**). Corresponding relative error for EIA approach in calculation of effective index (**b**) and cut-off width (**c**).

Let us now consider the propagation properties of rib waveguides with various values of the total height h parameter and constant ridge height $h_2 = h - h_1$ = 0.05 µm , see Figure 5a–c. Again, with the use of EIA, we can correctly predict single-mode conditions for rib waveguides realized in the SiO_2:TiO_2 platform, see Figure 5a. Additionally, as presented previously, the low difference between total and surrounding layer heights allows us to obtain almost negligible effective index error, i.e., below 0.1%, and lower multimodal cut-off error, i.e., below 16%, for all considered parameters, see Figure 5b,c. Moreover, the analysis presented in this work has revealed a weakly guided mode in the rib waveguide of height h = 0.275 µm, which preserves single-mode propagation within a wide range of waveguide widths, i.e., from 1.5 to almost 5.5 µm, and may be potentially applied as a good candidate for curved waveguides.

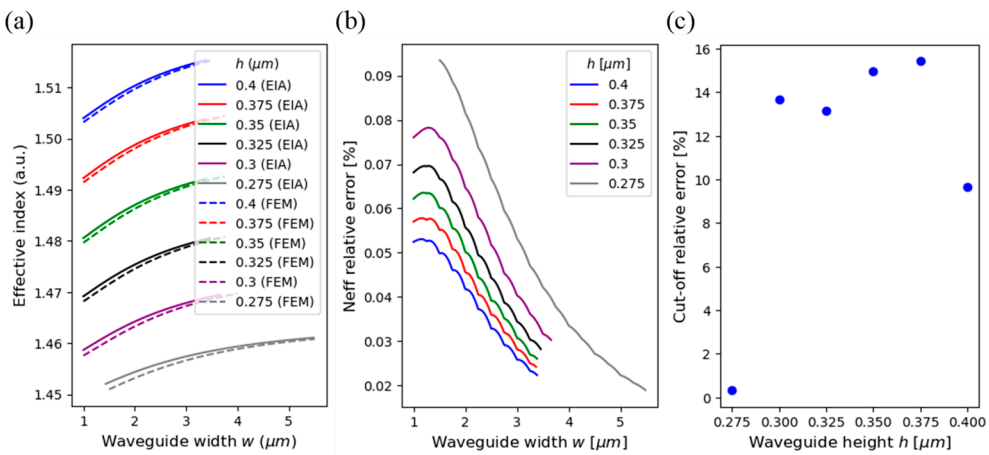

Figure 5. Effective index vs. waveguide width for rib waveguide of different total height, where solid curve corresponds to semi-analytical and dashed to numerical calculations (**a**). Corresponding relative errors for EIA approach in calculation of effective index (**b**) and cut-off width (**c**).

To validate our analysis of single-mode conditions, we demonstrate the normalized electric field distribution of modes existing in two rib waveguides of the same width w = 4.5 µm and different heights, i.e., $h = 0.275$ m (Figure 6a) and h = 0.4 µm (Figure 6b–d), which has been acquired with COMSOL 6.2 software. It can be observed that the waveguide of height h = 0.275 µm supports only single mode propagation for the given width, whilst the waveguide with h = 0.4 µm supports three modes in total, i.e., TE_0, TM_0 and TE_1,

which confirms previously obtained results (compare Figure 6a–d with Figure 5a). At this point, it is worth reiterating that the description of waveguides via the EIA approach is limited to waveguides with $h_1 < 0.5 * h$. Since the single-mode propagation for light of λ_0 = 0.633 µm in the SiO_2:TiO_2 rib waveguide is only possible for $h_1 < 0.5 * h$, which is why we have limited our analysis to λ_0 = 1.55 µm.

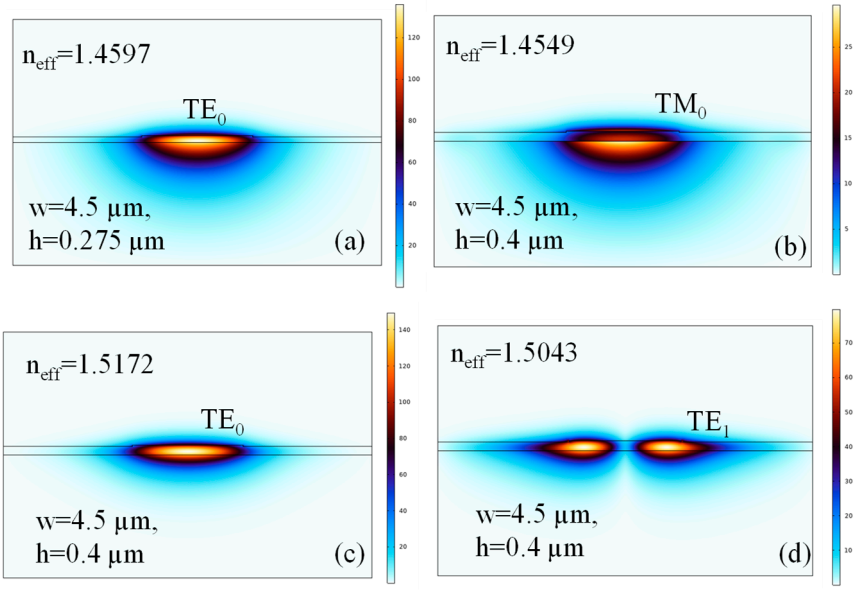

Figure 6. Normalized E-field distribution in the rib waveguide of dimensions supporting, (**a**) only TE_{00} mode, (**b**–**d**) supporting TM_0, TE_0 and TE_1 modes.

3.2. Ridge Waveguides

So far, we have established the applicability of the presented semi-analytical approach to describe propagation in rib waveguides. However, the prevalent integrated optics systems predominantly employ rectangular ridge waveguides. In this section, we extend our analysis to encompass the propagation properties of ridge waveguides with varying heights (h). Given that light propagation in SiO_2:TiO_2 waveguide systems can be achieved across visible and infrared spectral ranges, we explore two distinct wavelengths to offer representative examples for both optical bands: λ = 633 nm (n_f = 1.80321, n_s = 1.4570) and λ = 1550 nm (n_f = 1.75645, n_s = 1.4440). By using the proposed analytical method, it is possible to calculate effective indices for the considered parameters and wavelengths, see Figure 7a,d. The relative error for effective index estimation is still relatively low and does not exceed 2.25% for $\lambda = 633$ nm and 0.01% for $\lambda = 1550$ nm, while the relative error for determination of multimodal cut-off is significantly below 13.0% for $\lambda = 633$ nm and 3.75% for $\lambda = 1550$ nm. Furthermore, it can be observed that the presented method reveals a much lower average error for longer wavelengths, compared to Figure 7b,c and Figure 7e,f and for ridge waveguides rather than rib waveguides, compared to Figure 4b,c and Figure 7b,c.

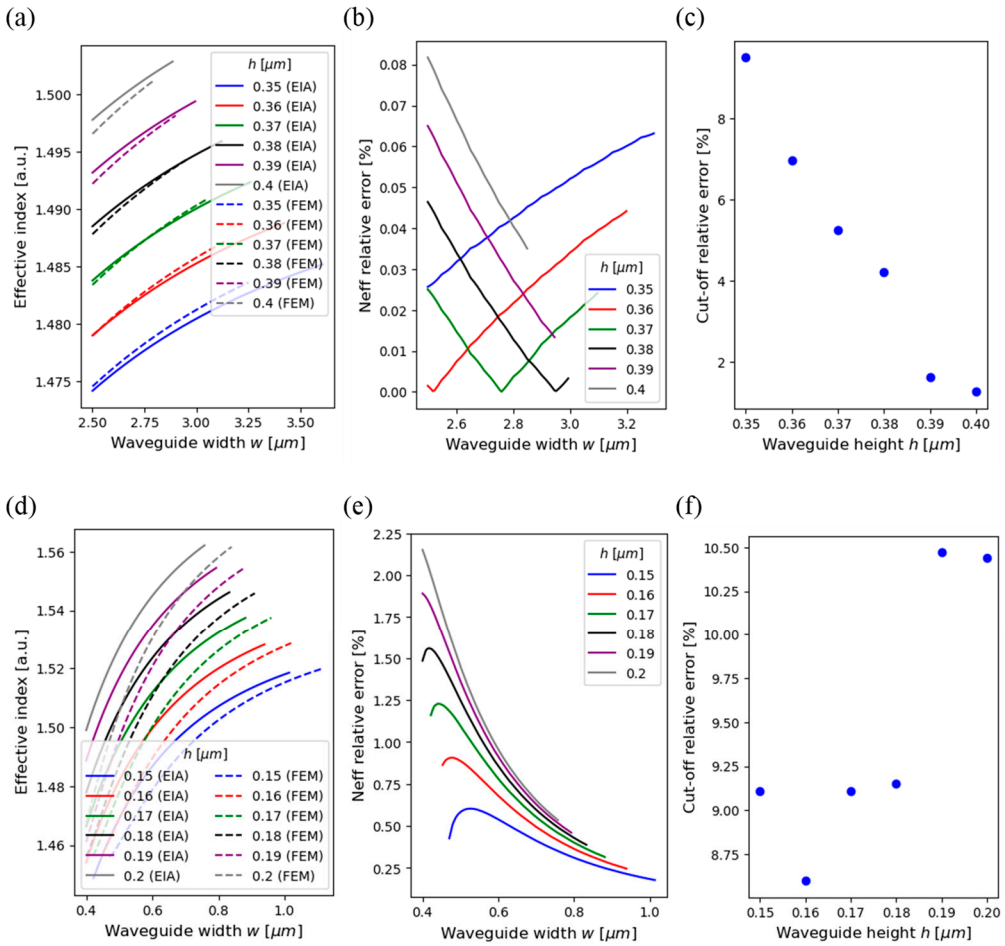

Figure 7. Effective index vs. waveguide width for ridge waveguide of different total height, where solid curve corresponds to semi-analytical and dashed to numerical calculations for $\lambda = 633$ (**a**) and $\lambda = 1550$ nm (**b**). Corresponding relative errors for the EIA approach in the calculation of effective index (**c**,**d**) and cut-off width (**e**,**f**).

In a manner analogous to the examination of rib waveguides, we illustrate the electric field distribution for two ridge waveguides with arbitrarily selected heights—specifically, h = 0.35 µm (Figure 8a) and h = 0.4 µm (Figure 8b,c). Both waveguides possess a uniform width of w = 3.2 µm, propagating light with a wavelength of λ = 1550 nm. Notably, the analysis reveals that single-mode propagation is exclusively sustained in the waveguide with h = 0.35 µm. Conversely, the waveguide with h = 0.4 µm fails to meet the conditions required for single-mode propagation. This observation reaffirms the consistency of our results obtained through the EIA approach, underscoring the validity of the findings (cf. Figure 8 with Figure 7a).

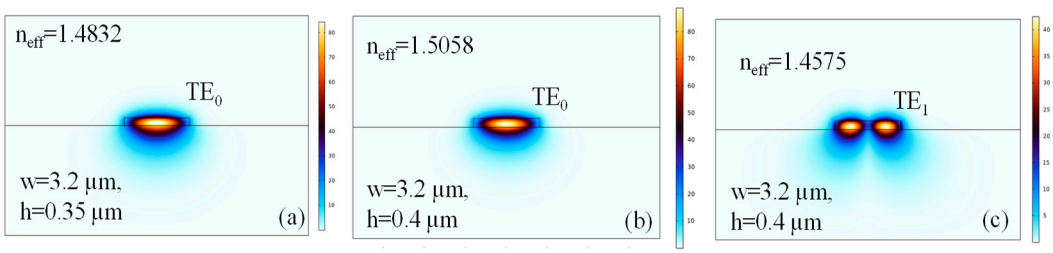

Figure 8. Normalized E-field distribution in the ridge waveguide of dimensions supporting, (**a**) only TE_0 mode, (**b**,**c**) TE_0 and TE_1 modes.

3.3. EIA vs. FEM: Discussion

Despite the innate limitations of the approximate method, the conducted analysis allows us to confirm that EIA may be applied to determine effective index and single-mode propagation conditions for rib and ridge waveguides with reasonable error. Still, EIA is not able to deliver results as accurate as FEM, which may be treated as an exact solution. However, the main advantage of applying EIA lies in the possibility of performing complex and multi-parameter computations with almost instant execution time. Tables 1 and 2 contain a comparison between simulation parameters and computational time for EIA and FEM.

Table 1. Computational time of rib and ridge waveguide via FEM.

Waveguide Type	Computational Domain	Mesh Size of the Core	Mesh Size of Air and Substrate	Computational Parameters	Total Computational Time
Rib	15 µm × 10 µm	$\lambda/20$	$\lambda/10$	Figure 5a	30 min 34 s
Ridge	15 µm × 10 µm	$\lambda/20$	$\lambda/10$	Figure 7a	22 min 54 s

Table 2. Computational time of rib and ridge waveguide via EIA.

Waveguide Type	Total Simulation Points	Computational Parameters	Averaged Computational Time per Point	Total Computational Time
Rib	1500	Figure 5a	~415 µs	~0.62 s
Ridge	1500	Figure 7a	~304 µs	~0.46 s

Examining Tables 1–3, it becomes evident that the EIA approach, while maintaining a commendably low error margin, yields results with remarkable speed in contrast to the FEM. The entire computational process utilizing the EIA can be accomplished in under a second. This significant reduction in calculation time not only expedites the overall analysis but also opens avenues for exploring a more intricate parameter space. This acceleration is particularly advantageous in the development of new functional blocks, where a comprehensive exploration of diverse parameters is often essential.

Table 3. Averaged error of EIM method.

Waveguide Type	Computational Parameters	Average Neff Error	Average Cut-Off Error
Rib	Figure 5b,c	~0.11%	~18.27%
Rib	Figure 6b,c	~0.047%	~11.2%
Ridge	Figure 7b,c	~0.033%	~4.8%
Ridge	Figure 7e,f	~0.79%	~9.5%

4. Conclusions

This study introduces a semi-analytical approximate method designed for the calculation of the effective index of modes and the determination of single-mode conditions in rectangular waveguides where an exact analytical solution is unattainable. The key strengths of this approach lie in its straightforward implementation, adaptability to various geometries, and notably rapid computation times compared to numerical solvers. A single point of calculation is executed within a few hundred microseconds, contrasting with typical numerical solvers that demand seconds for the same task. The accelerated result delivery of this proposed approach facilitates its application in multiparameter sweep simulations, enabling the characterization of a given technology, waveguide geometry, or material platform. This expeditious analysis serves as a valuable foundation for subsequent,

more detailed numerical simulations, contributing to a more comprehensive understanding of the system under consideration.

As an example, we have considered rib and ridge waveguides realized on the silica-titania technological platform that was developed in the frame of our project. Additionally, we have performed calculations for two different wavelengths that are supported in the considered material platform, i.e., $\lambda = 633$ nm and $\lambda = 1550$ nm, and a wide range of geometrical parameters, which allows calculating effective modal indices and estimating conditions for single-mode propagation in the considered waveguides. All obtained analytical results have been confirmed with numerical calculations obtained via the use of COMSOL 6.2 software. It is essential to emphasize that the presented method is not confined solely to the silica-titania platform. Its versatility allows for straightforward application to various materials, and with further adjustments, it can be extended to accommodate waveguides of diverse geometries. These may include strip-loaded or buried waveguides, as well as alterations for core mediums, such as anisotropic or metamaterial waveguides. This adaptability underscores the broad applicability of the method across different materials and waveguide configurations, enhancing its utility in a range of photonic applications.

Despite inherent limitations of approximation-based methods, such as error in determining single mode cut-off error or limited applicability in the case of rib waveguides, the presented semi-analytical method excels in rapidly generating results, providing a foundation for subsequent design processes. We firmly believe that this approach can function as a dependable and expeditious tool, particularly during the preliminary stages of designing functional blocks for both emerging and established PIC technologies.

Author Contributions: Conceptualization, B.J. and M.A.B.; methodology, B.J.; software, M.A.B.; validation, B.J. and M.A.B.; formal analysis, B.J.; investigation, B.J. and M.A.B.; resources, R.P.; data curation, B.J.; writing—original draft preparation, B.J. and M.A.B.; writing—review and editing, B.J., M.A.B. and R.P.; visualization, M.A.B.; supervision, R.P.; project administration, R.P.; funding acquisition, M.A.B. All authors have read and agreed to the published version of the manuscript.

Funding: This research received no external funding.

Data Availability Statement: Data are contained within the article.

Acknowledgments: The authors acknowledge the constant support of the Warsaw University of Technology in the completion of this work.

Conflicts of Interest: The authors declare no conflict of interest.

References

1. Miller, D. Optical interconnects to silicon. *IEEE J. Sel. Top. Quantum Electron.* **2000**, *6*, 1312–1317. [CrossRef]
2. Sun, C.; Wade, M.T.; Lee, Y.; Orcutt, J.S.; Alloatti, L.; Georgas, M.S.; Waterman, A.S.; Shainline, J.M.; Avizienis, R.R.; Lin, S.; et al. Single-chip microprocessor that communicates directly using light. *Nature* **2015**, *528*, 534–538. [CrossRef] [PubMed]
3. Atabaki, A.H.; Moazeni, S.; Pavanello, F.; Gevorgyan, H.; Notaros, J.; Alloatti, L.; Wade, M.T.; Sun, C.; Kruger, S.A.; Meng, H.; et al. Integrating photonics with silicon nanoelectronics for the next generation of systems on a chip. *Nature* **2018**, *556*, 349–354. [CrossRef] [PubMed]
4. Liu, W.; Li, M.; Guzzon, R.S.; Norberg, E.J.; Parker, J.S.; Lu, M.; Coldren, L.A.; Yao, J. A fully reconfigurable photonic integrated signal processor. *Nat. Photonics* **2016**, *10*, 190–195. [CrossRef]
5. Arafin, S.; Coldren, L.A. Advanced InP Photonic Integrated Circuits for Communication and Sensing. *IEEE J. Sel. Top. Quantum Electron.* **2018**, *24*, 1–12. [CrossRef]
6. Heck, M.J.R. Highly integrated optical phased arrays: Photonic integrated circuits for optical beam shaping and beam steering. *Nanophotonics* **2017**, *6*, 93–107. [CrossRef]
7. Elshaari, A.W.; Pernice, W.; Srinivasan, K.; Benson, O.; Zwiller, V. Hybrid integrated quantum photonic circuits. *Nat. Photonics* **2020**, *14*, 285–298. [CrossRef]
8. Gemma, L.; Bernard, M.; Ghulinyan, M.; Brunelli, D. Analysis of control and sensing interfaces in a photonic integrated chip solution for quantum computing. In Proceedings of the 17th ACM International Conference on Computing Frontiers, Catania, Italy, 11–13 May 2020; pp. 245–248. [CrossRef]
9. Cole, C.; Huebner, B.; Johnson, J.E. Photonic integration for high-volume, low-cost applications. *IEEE Commun. Mag.* **2009**, *47*, S16–S22. [CrossRef]

10. Kish, F.A.; Welch, D.; Nagarajan, R.; Pleumeekers, J.L.; Lal, V.; Ziari, M.; Nilsson, A.; Kato, M.; Murthy, S.; Evans, P.; et al. Current Status of Large-Scale InP Photonic Integrated Circuits. *IEEE J. Sel. Top. Quantum Electron.* **2011**, *17*, 1470–1489. [CrossRef]
11. Klamkin, J.; Zhao, H.; Song, B.; Liu, Y.; Isaac, B.; Pinna, S.; Sang, F.; Coldren, L. Indium Phosphide Photonic Integrated Circuits: Technology and Applications. In Proceedings of the 2018 IEEE BiCMOS and Compound Semiconductor Integrated Circuits and Technology Symposium (BCICTS), San Diego, CA, USA, 15–17 October 2018; pp. 8–13. [CrossRef]
12. Helkey, R.; Saleh, A.A.M.; Buckwalter, J.F.; Bowers, J.E. High-Performance Photonic Integrated Circuits on Silicon. *IEEE J. Sel. Top. Quantum Electron.* **2019**, *25*, 1–15. [CrossRef]
13. Pelli, S.; Righini, G.C.; Scaglione, A.; Guglielmi, M.; Martucci, A. Direct laser writing of ridge optical waveguides in silica-titania glass sol-gel films. *Opt. Mater.* **1996**, *5*, 119–126. [CrossRef]
14. Roy, R.D.; Sil, D.; Jana, S.; Biswas, P.K.; Bhadra, S.K. Experimental study of perfectly patterned silica-titania optical waveguide. *Photonics Sens.* **2012**, *2*, 81–91. [CrossRef]
15. Royer, F.; Jamon, D.; Rousseau, J.J.; Roux, H.; Zins, D.; Cabuil, V. Magneto-optical nanoparticle-doped silica-titania planar waveguides. *Appl. Phys. Lett.* **2005**, *86*, 011107. [CrossRef]
16. Karasiński, P. Embossable grating couplers for planar evanescent wave sensors. *Opto-Electron. Rev.* **2011**, *19*, 10–21. [CrossRef]
17. Butt, M.A.; Tyszkiewicz, C.; Karasiński, P.; Zięba, M.; Hlushchenko, D.; Baraniecki, T.; Kazmierczak, A.; Piramidowicz, R.; Guzik, M.; Bachmatiuk, A. Development of a low-cost silica-titania optical platform for integrated photonics applications. *Opt. Express* **2022**, *30*, 23678–23694. [CrossRef] [PubMed]
18. Doerr, C.R. Photonic Integrated Circuits for High-Speed Communications. In Proceedings of the Conference on Lasers and Electro-Optics, San Jose, CA, USA, 16–21 May 2010; p. CFE3. [CrossRef]
19. Jans, H.; O'Brien, P.; Artundo, I.; Hoofman, R.; Geuzebroek, D.; Dumon, P.; van der Vliet, M.; Witzens, J.; Bourguignon, E.; Van Dorpe, P.; et al. Integrated bio-photonics to revolutionize health care enabled through PIX4life and PIXAPP. In Proceedings of the Nanoscale Imaging, Sensing, and Actuation for Biomedical Applications XV, San Francisco, CA, USA, 27 January–1 February 2018; pp. 98–102. [CrossRef]
20. Photonic Integrated Circuit Based Sensing Modules with Hybrid Integration in the Silicon Nitride TriPleXTM Platform. Available online: https://opg.optica.org/abstract.cfm?uri=ofc-2019-Tu2D.4 (accessed on 14 December 2023).
21. Giordani, T.; Hoch, F.; Carvacho, G.; Spagnolo, N.; Sciarrino, F. Integrated photonics in quantum technologies. *Riv. Nuovo Cimento* **2023**, *46*, 71–103. [CrossRef]
22. Martin, A.; Verheyen, P.; De Heyn, P.; Absil, P.; Feneyrou, P.; Bourderionnet, J.; Dodane, D.; Leviandier, L.; Dolfi, D.; Naughton, A.; et al. Photonic Integrated Circuit-Based FMCW Coherent LiDAR. *J. Light. Technol.* **2018**, *36*, 4640–4645. [CrossRef]
23. Goell, J.E. A Circular-Harmonic Computer Analysis of Rectangular Dielectric Waveguides. *Bell Syst. Tech. J.* **1969**, *48*, 2133–2160. [CrossRef]
24. Marcatili, E.A.J. Dielectric Rectangular Waveguide and Directional Coupler for Integrated Optics. *Bell Syst. Tech. J.* **1969**, *48*, 2071–2102. [CrossRef]
25. Kogelnik, H. Theory of Dielectric Waveguides. In *Integrated Optics*; Tamir, T., Ed.; Topics in Applied Physics; Springer: Berlin/Heidelberg, Germany, 1975; Volume 7, pp. 13–81. [CrossRef]
26. Butt, M.A.; Kaźmierczak, A.; Tyszkiewicz, C.; Karasiński, P.; Środa, E.; Olszewski, J.; Pala, P.; Martynkien, T.; Hlushchenko, D.; Baraniecki, T.; et al. HYPHa project: A low-cost alternative for integrated photonics. *Photonics Lett. Pol.* **2022**, *14*, 25–27. [CrossRef]
27. Malitson, I.H. Interspecimen comparison of the refractive index of fused silica. *J. Opt. Soc. Am.* **1965**, *55*, 1205–1209. [CrossRef]
28. Karasiński, P.; Tyszkiewicz, C.; Domanowska, A.; Michalewicz, A.; Mazur, J. Low loss, long time stable sol–gel derived silica–titania waveguide films. *Mater. Lett.* **2015**, *143*, 5–7. [CrossRef]
29. Ciddor, P.E. Refractive index of air: New equations for the visible and near infrared. *Appl. Opt.* **1996**, *35*, 1566–1573. [CrossRef]

Disclaimer/Publisher's Note: The statements, opinions and data contained in all publications are solely those of the individual author(s) and contributor(s) and not of MDPI and/or the editor(s). MDPI and/or the editor(s) disclaim responsibility for any injury to people or property resulting from any ideas, methods, instructions or products referred to in the content.